The Astrophysical Journal, 966:203 (13pp), 2024 May 10 https://doi.org/10.3847/1538-4357/ad3075
© 2024. The Author(s). Published by the American Astronomical Society.
OPEN ACCESS

Evolution of Subsonic Shock Waves Associated with Reconnection Jets in Earth's Magnetotail

Kuldeep Singh[1,2], Frank Verheest[3,4], and Ioannis Kourakis[1,2]
[1] Space and Planetary Science Center, Khalifa University, Abu Dhabi, UAE; singh.kdeep07@gmail.com, kuldeep.singh@ku.ac.ae
[2] Department of Mathematics, Khalifa University of Science & Technology, Abu Dhabi, UAE
[3] Sterrenkundig Observatorium, Universiteit Gent, Ghent, Belgium
[4] School of Chemistry and Physics, University of KwaZulu-Natal, Pietermaritzburg, South Africa
Received 2024 January 25; revised 2024 March 4; accepted 2024 March 4; published 2024 May 8

Abstract

Motivated by the signatures of nonlinear electrostatic waves observed by the Magnetospheric Multiscale spacecraft mission in reconnection jet regions of Earth's magnetotail, we have explored the dynamical features of ion-acoustic shock waves in the magnetotail. In this investigation, we have examined the dynamics and characteristics of ion-acoustic subsonic shock waves in non-Maxwellian space plasma comprising of two counterstreaming ion beams with suprathermal electrons, assumed to follow a kappa (κ) distribution. A reductive perturbation technique has been adopted to establish an evolution equation for small amplitude electrostatic shock structures. Importantly, subsonic waves only exist when the beam velocity exceeds a certain threshold, beyond which supersonic and subsonic waves may coexist. The combined effects of the beam velocity and the non-Maxwellian electron statistics have been analyzed to examine the characteristics of subsonic shock waves. Both symmetric and asymmetric (in relative beam density) models have been considered, leading to distinct possibilities in the evolution of subsonic shock waves. The findings of the investigation will help unfold the relatively unexplored dynamical characteristics of subsonic shock waves that may form and propagate in the magnetosphere.

Unified Astronomy Thesaurus concepts: Plasma physics (2089); Space plasmas (1544)

1. Introduction

Nonlinear electrostatic waves have been routinely detected in Earth's magnetosphere by various spacecraft missions, including Viking (Boström et al. 1988), Geotail (Matsumoto et al. 1994), FAST (Ergun et al. 1998), and Cluster (Pickett et al. 2004) among others. Analogous localized electrostatic structures (electrostatic solitary waves, ESWs) have been observed by planetary missions like Cassini and MAVEN in the magnetospheres of Saturn (Pickett et al. 2015) and Mars (Andersson et al. 2015; Kakad et al. 2022), respectively. From a modeling perspective, the fundamental analytical tools for studying these waves were initially developed by Sagdeev (1966) and Washimi & Taniuti (1966). In recent years, numerous theoretical and experimental investigations have concentrated on solitary waves (SWs) occurring in different plasma contexts; see e.g., the studies by Baboolal et al. (1990), Berthomier et al. (1998), Hellberg & Verheest (2008), Verheest & Hellberg (2009), Lakhina et al. (2011), Mahmood & Ur-Rehman (2013), and Ur-Rehman et al. (2014). Subsequently, simulation studies have explored SWs within multicomponent plasmas (Kakad et al. 2016; Singh et al. 2020, 2021, 2022).

The investigation of shock waves in collisionless plasmas has garnered significant attention over recent decades, both from experimental (Nakamura et al. 1999; Heinrich et al. 2009) and theoretical (Washimi & Taniuti 1966; Malfliet & Hereman 1996; Kourakis et al. 2012a, 2012b; Sultana et al. 2012) perspectives. The increasing level of detail provided by both laboratory measurements and space-based observations underscores the necessity for continuous refinement of the underlying theoretical framework. Many theoretical investigations in the literature have relied on either the Burgers equation or the hybrid Korteweg–de Vries–Burgers (KdVB) equation, which elegantly captures the intricate interplay between nonlinearity, dispersion, and dissipation effects in the generation and evolution of shock structures. Nonetheless, the diverse range of plasma environments where shock waves may arise has posed challenges in developing a unified theoretical description for these inherently nonlinear phenomena.

The presence of both fast and slow ion-acoustic (IA) modes has been confirmed in multi-ion (warm ion) plasma models utilizing linear wave theory, subsequently leading to intriguing nonlinear investigations of plasmas permeated by two opposing ion-beam flows (Lakhina et al. 2020; Verheest & Hellberg 2021). These studies, employing a multi-plasma-fluid framework, have revealed that beam-permeated plasmas may sustain not just the "traditional" supersonic electrostatic solitary wave structures, but also a subsonic IA nonlinear mode. This subsonic mode propagates at a velocity lower than the speed of sound but above a specific threshold (for the Mach number value), say $M_{\rm min}$ (Lakhina et al. 2020; Verheest & Hellberg 2021). A noteworthy development is the observation that the amplitude of SWs demonstrates an intriguing growth trend as the Mach number decreases toward the critical value of $M_{\rm min}$, below which the existence of SWs becomes unfeasible. A recent study by Lakhina et al. (2021) proceeded further by investigating the generation mechanism of these waves in the context of reconnection jets. This investigation considered the influence of beam thermal effects, an aspect not covered in a prior study by Liu et al. (2019). That study assumed the presence of ion beams coexisting with Maxwellian electrons within the background plasma.

Lakhina et al. (2020, 2021) employed a plasma-fluid model that featured two counterstreaming ion beams and Maxwellian

Original content from this work may be used under the terms of the Creative Commons Attribution 4.0 licence. Any further distribution of this work must maintain attribution to the author(s) and the title of the work, journal citation and DOI.

electrons. They were pioneers in demonstrating the possibility of SWs existing at Mach numbers below a critical threshold, provided that specific criteria were satisfied. In a subsequent study, Verheest & Hellberg (2021) re-examined this same model, omitting thermal ion effects and shedding light on the pivotal role played by the velocity of the ion beams, rather than thermal factors, in the formation of subsonic SWs. Their meticulous investigation conclusively verified that these slow-mode SWs indeed propagate at subsonic speeds in the laboratory frame, both in symmetric and asymmetric beam-plasma models.

Various satellite missions have provided compelling evidence for the prevalence of energetic particles in a variety of space and astrophysical settings. In these scenarios, the electron velocity distribution exhibits a distinctive long-tailed pattern at high energies, giving rise to a significant suprathermal component. This distribution diverges from the conventional "textbook" model of a thermal Maxwell–Boltzmann distribution, as discussed by Livadiotis (2017, 2018). Suprathermal particles have been documented in various locations, including Earth's magnetosphere (Feldman et al. 1975) and the auroral region (Mendis & Rosenberg 1994; Lazar et al. 2008), as well as in Mercury's magnetosphere, i.e., detected by MESSENGER mission data (Ho et al. 2011). The kappa distribution was initially introduced by Vasyliunas (1968) as a heuristic model to interpret data from OGO 1 and OGO 3 spacecraft within Earth's magnetosphere. Subsequently, kappa-type (non-Maxwellian) distribution functions have been applied to characterize suprathermal particle populations in the solar wind (Armstrong et al. 1983) and in planetary magnetospheres, e.g., Earth's, Saturn's, and Jupiter's (Leubner 1982; Singh et al. 2021, 2022, 2023; Varghese et al. 2023).

Magnetic reconnection is a mechanism through which magnetic energy is converted into plasma kinetic energy, accompanied by changes in the magnetic field configuration (Yamada et al. 2010; Fu et al. 2017). In Earth's magnetotail, this process occurs when two oppositely directed plasmas become interconnected with magnetic field lines, leading to the ejection of these reconnected plasmas at high velocities from the reconnection site. This phenomenon is commonly referred to as a reconnection jet (Cao et al. 2013). It is now well-established that reconnection jets play a pivotal role in energizing plasmas in space and astrophysical contexts, including phenomena like solar flares, pulsar winds, and active galactic nuclei (Kirk & Skjaeraasen 2003; Chen et al. 2019; Liu et al. 2019; Lakhina et al. 2021). Within Earth's magnetotail, reconnection jets can give rise to various types of plasma waves and instabilities, in addition to ESWs. Liu et al. (2019) presented the first observational evidence, using data from the Magnetospheric Multiscale (MMS) spacecraft, that elucidated the development of ESWs associated with cold ion beams within reconnection jets in Earth's magnetotail.

The magnetotail region is extensively permeated by counter-streaming ion beams, exhibiting relative velocities of up to $2000\,\mathrm{km\,s^{-1}}$, in conjunction with hot electrons. These ion beams, as highlighted in the study by Liu et al. (2019), can serve as a source of free energy, contributing to the generation of ESWs. Over the past decade, slow IA electron SWs have been documented within the plasma sheet boundary layer (Norgren et al. 2015) and at reconnection sites (Graham et al. 2015). More recently, Lakhina et al. (2021) investigated the formation of both fast and slow ESWs within reconnection jets, taking into account the presence of two ion beams, thermal effects, and Maxwellian electrons, as mentioned above.

The research presented in this paper was initiated in response to the aforementioned factors and marked an inaugural (unprecedented, to the best of our knowledge) investigation of subsonic shock waves within the reconnection jet region(s) of Earth's magnetotail (plasma). Such subsonic shocks were previously detected by various satellite observations (Zhou et al. 2018; Gingell et al. 2019), but the underlying theoretical setting has so far remained unexplored in the existing scientific literature. Motivated by these considerations, our study at hand focuses on the presence of two counterstreaming (cold) ion populations surrounded by suprathermal electrons. To identify and characterize the plasma regime(s) where subsonic shock waves may exist, our approach in this article relies on a nonlinear reductive perturbation technique, specifically the KdVB equation, as our main analytical tool.

To the best of our knowledge, this investigation represents a novel endeavor as it concentrates on a realistic scenario within space plasmas to predict subsonic shock-like structure occurrence. Specifically, we explore the collision of two counterstreaming plasmas in the presence of nonthermal (kappa-distributed) electrons, a prevalent condition widely observed in Earth's magnetosphere. This phenomenon may also have relevance in planetary magnetospheres (e.g., the Martian one) influenced by interactions with the solar wind, which serves as a continuous source of streaming ions and energized electrons. Previous research primarily centered on supersonic SWs, with subsonic wave solutions typically ruled out in a quiescent plasma without a beam (Dubinov 2009).

2. A Double Beam Plasma Model

We have considered a plasma consisting of non-Maxwellian electrons (mass m_e, charge $-e$) and double ion-beam fluids (mass $m_1 = m_2 = m_i$, charge $q_1 = q_2 = +e$. (We have considered a charge state $Z_i = +1$ as we are dealing with proton beams, i.e., hydrogen nuclei.)

The fluid model equations describe the plasma state in terms of the two proton fluid densities (n_j) and the fluid speeds (u_j)—where $j = 1$ or 2, respectively, for each of the two proton fluids—consist of the continuity equation(s):

$$\frac{\partial \tilde{n}_j}{\partial \tilde{t}} + \frac{\partial (\tilde{n}_j \tilde{u}_j)}{\partial \tilde{x}} = 0, \tag{1}$$

the momentum equation(s):

$$\frac{\partial \tilde{u}_j}{\partial \tilde{t}} + \tilde{u}_j \frac{\partial \tilde{u}_j}{\partial \tilde{x}} = -\frac{e}{m_i}\frac{\partial \tilde{\phi}}{\partial \tilde{x}} + \tilde{\eta}_j \frac{\partial^2 \tilde{u}_j}{\partial \tilde{x}^2}, \tag{2}$$

and Poisson's equation:

$$\frac{\partial^2 \tilde{\phi}}{\partial \tilde{x}^2} = -\frac{e}{\epsilon_0}(\tilde{n}_1 + \tilde{n}_2 - \tilde{n}_e), \tag{3}$$

where $\tilde{\phi}$ is the electrostatic potential and ϵ_0 is the permittivity of vacuum.

The electron density entering Poisson's equation can be obtained by integrating the kappa velocity distribution

(Hellberg et al. 2009) as

$$\tilde{n}_e = n_{e,0}\left(1 - \frac{e\tilde{\phi}}{k_B T_e\left(\kappa - \frac{3}{2}\right)}\right)^{-\kappa+\frac{1}{2}}. \quad (4)$$

At equilibrium, the charge neutrality condition is

$$n_{e,0} = n_0 = n_{1,0} + n_{2,0}, \quad (5)$$

where n_j for $(j = 1 \text{ or } 2)$ denote(s) the unperturbed number density of the ions, respectively.

For the sake of analytical convenience, we shall adopt the following normalization: $n_j = \tilde{n}_j/n_0$, $n_e = \tilde{n}_e/n_0$, $u_j = \tilde{u}_j/\mathrm{C}_0$ (where $\mathrm{C}_0 = (k_B T_e/m_i)^{1/2}$ is the IA/sound speed in (single) ion-electron plasma), $\phi = e\tilde{\phi}/(k_B T_e)$, $x = \tilde{x}/\lambda_{D,e}$ (where $\lambda_{D,e} = (\epsilon_0 k_B T_e/(e^2 n_0))^{1/2}$ is a characteristic length inspired by the expression for the Debye length in electron-ion (e-i) plasma), and $t = \omega_{p,i}\tilde{t}$ (where $\omega_{p,i} = [e^2 n_0/(\epsilon_0 m_i)]^{1/2}$ adopts the expression for the ion plasma frequency in e-i plasma). Furthermore, the ion viscosity is rescaled as $\eta_j = \tilde{\eta}_j/(\lambda_{De}^2 \omega_{p,i})$, while the drifting speed of the two ion fluids (i.e., the beams) is also normalized as $u_{j,0} = \tilde{u}_{j,0}/\mathrm{C}_0$.

Applying the above normalization scheme, Equations (1)–(4) take the form

$$\frac{\partial n_j}{\partial t} + \frac{\partial (n_j u_j)}{\partial x} = 0, \quad (6)$$

$$\frac{\partial u_j}{\partial t} + u_j \frac{\partial u_j}{\partial x} = -\frac{\partial \phi}{\partial x} + \eta_j \frac{\partial^2 u_j}{\partial x^2}, \quad (7)$$

$$\frac{\partial^2 \phi}{\partial x^2} = n_e - \delta_1 n_1 - \delta_2 n_2, \quad (8)$$

where

$$n_e = \left(1 - \frac{\phi}{\kappa - \frac{3}{2}}\right)^{-\kappa+\frac{1}{2}} \approx 1 + c_1\phi + c_2\phi^2 + ... \quad (9)$$

where

$$c_1 = \frac{\kappa - 1/2}{\kappa - 3/2} \quad \text{and} \quad c_2 = \frac{\kappa^2 - 1/4}{2(\kappa - 3/2)^2}.$$

Note that charge neutrality at equilibrium imposes the condition:

$$\delta_1 + \delta_2 = 1,$$

where $\delta_1 = \frac{n_{1,0}}{n_0}$ and $\delta_2 = \frac{n_{2,0}}{n_0}$ reflect the relative density ratio (with respect to the total ion density n_0) of the ion beams.

3. Linear Analysis

Before examining the nonlinear analysis of IA waves, we will study the linear stability briefly. By linearizing Equations (6)–(9) and assuming harmonic oscillations of angular frequency ω and wavenumber k, we obtain the linear dispersion relation

$$\frac{k^2\delta_1}{(\omega - ku_{1,0})^2} + \frac{k^2\delta_2}{(\omega - ku_{2,0})^2} = k^2 + \frac{\kappa - \frac{1}{2}}{\kappa - \frac{3}{2}}. \quad (10)$$

This is a fourth-order polynomial equation, which gives two fast and two slow modes. In the limiting case, without streaming velocities, i.e., $u_{1,0} = u_{2,0} = 0$, the above relation becomes

$$\omega_0^2 = \frac{k^2}{k^2 + c_1}, \quad (11)$$

where c_1 was defined above. Note that the quantity c_1 is related to both the (kappa-dependent) charge screening length λ_{Debye} and sound speed C_s in suprathermal e-i plasmas, both of which scale as $\lambda_{\mathrm{Debye}}, \mathrm{C}_s \sim 1/\sqrt{c_1}$, as discussed by Kourakis et al. (2012a) and independently (for the Debye length) by Bryant (1996) and Livadiotis & McComas (2014). (As expected, c_1 tends to unity in the Maxwellian limit as $\kappa \to \infty$).

Equation (10) has four roots, thus prescribing two fast IA modes (in addition to two slow modes), which in fact propagate in opposite directions, i.e., one propagates toward the right and the other one toward the left.

Inspired by the analysis in Lakhina et al. (2020) and Verheest & Hellberg (2021), we may now proceed by assuming a symmetric bi-ion plasma, i.e., $\delta_1 = \delta_2 = \delta = 1/2$, with $u_{1,0} = -u_0$, and $u_{2,0} = u_0$. Substituting into the above dispersion relation, we are led to

$$\omega^4 - (\omega_0^2 + 2k^2u_0^2)\omega^2 - k^2u_0^2(\omega_0^2 - k^2u_0^2) = 0 \quad (12)$$

and the corresponding solutions are given by

$$\omega_{F,S}^2 = \frac{\omega_0^2}{2}[1 + 2(k^2 + c_1)u_0^2 \pm \sqrt{1 + 8(k^2 + c_1)u_0^2}]. \quad (13)$$

The subscripts F and S denote the fast and slow IA modes corresponding to the $\pm$ sign, respectively. A short algebraic calculation reveals that there is a threshold value in the beam velocity above which subsonic IA waves exist, while the interval below is an unstable region. This was discussed in recent work by Singh et al. (2023; see Figures 1–3 therein).

4. Nonlinear Analysis

The standard reductive perturbative technique, as originally introduced by Washimi & Taniuti (1966) can be employed at this stage. The method relies on introducing (independent) stretching coordinates as

$$\xi = \epsilon^{\frac{1}{2}}(x - \lambda t) \quad \text{and} \quad \tau = \epsilon^{\frac{3}{2}}t, \quad (14)$$

where $\epsilon \ll 1$ is a small (real) parameter reflecting the strength of nonlinearity. Here, λ is the phase speed of the solution (wave, shock form), whose value is left to be determined later, eventually imposed by algebraic considerations. The dependent variables n_j, u_j, and ϕ can be expanded as a power of ϵ:

$$\begin{bmatrix} n_j \\ u_j \\ \phi \end{bmatrix} \approx \begin{bmatrix} 1 \\ u_{j,0} \\ 0 \end{bmatrix} + \epsilon \begin{bmatrix} n_{j,1} \\ u_{j,1} \\ \phi_1 \end{bmatrix} + \epsilon^2 \begin{bmatrix} n_{j,2} \\ u_{j,2} \\ \phi_2 \end{bmatrix} + ... \quad (15)$$

We have considered a weakly damped medium, assuming an infinitesimal (value of the) kinematic viscosity, as

$$\eta_j \approx \epsilon^{1/2}\eta_{j0}, \quad (16)$$

where η_{j0} is a finite quantity. The latter assumption is justified a posteriori by the fact that dispersive, nonlinear, and dissipative terms will arise on equal footing, in the perturbative analysis, at a certain order.

Substituting Equations (9)–(15) into Equations (6)–(8) leads to the following expressions, upon solving the first-order equations:

$$n_{j,1} = \frac{1}{(\lambda - u_{j,0})^2}\phi_1 \quad \text{and} \quad u_{j,1} = \frac{1}{\lambda - u_{j,0}}\phi_1. \tag{17}$$

An algebraic compatibility condition leads to the following expression for the wave phase speed λ:

$$\frac{\delta_1}{(\lambda - u_{j,0})^2} + \frac{\delta_2}{(\lambda - u_{j,0})^2} = \frac{\kappa - \frac{1}{2}}{\kappa - \frac{3}{2}}. \tag{18}$$

Note that the right-hand side (RHS) is equal to c_1 (essentially the signature of the kappa distribution in the linear results), which was defined previously. It is interesting to point out that, had one considered the dispersion relation (Equation (10)) in the infinite-wavelength (i.e., vanishing wavenumber) limit $k \to 0$, one would have found precisely Equation (18), via a different approach. One concludes, therefore, that parameter λ represents the phase speed of low-k linear waves, i.e., essentially the true IA ("sound") speed in the given plasma configuration, as physically and mathematically expected.

Proceeding to the next higher order of ϵ, one finds the following equations:

$$\frac{\partial n_{j,1}}{\partial t} - \lambda\frac{\partial n_{j,2}}{\partial \xi} + \frac{\partial u_{j,2}}{\partial \xi} + \frac{\partial}{\partial \xi}(n_{j,1}u_{j,1}) = 0, \tag{19}$$

$$\frac{\partial u_{j,1}}{\partial t} - \lambda\frac{\partial u_{j,2}}{\partial \xi} + u_{j,1}\frac{\partial u_{j,1}}{\partial \xi} = -\frac{\partial \phi_2}{\partial \xi} + \eta_{j,0}\frac{\partial^2 u_{j,1}}{\partial \xi^2}, \tag{20}$$

$$\frac{\partial^2 \phi_1}{\partial \xi^2} = c_1\phi_2 + c_2\phi_1^2 - \delta_1 n_{1,2} - \delta_2 n_{2,2}. \tag{21}$$

One may now eliminate the second-order quantities from Equations (19)–(21) by simply using Equations (17)–(18). After some straightforward algebraic manipulation, one obtains a closed partial-differential equation (PDE) in the form of a hybrid KdVB equation:

$$\frac{\partial \phi_1}{\partial t} + \mathrm{A}\phi_1\frac{\partial \phi_1}{\partial \xi} + \mathrm{B}\frac{\partial^3 \phi_1}{\partial \xi^3} = \mathrm{C}\frac{\partial^2 \phi_1}{\partial \xi^2}. \tag{22}$$

The coefficients appearing in the KdVB Equation (22) consist of the nonlinearity coefficient

$$\mathrm{A} = \mathrm{B}\left\{3\left[\frac{\delta_1}{(\lambda - u_{1,0})^4} + \frac{\delta_2}{(\lambda - u_{2,0})^4}\right] - 2c_2\right\}, \tag{23}$$

the dispersion coefficient

$$\mathrm{B} = \frac{1}{2}\left[\frac{\delta_1}{(\lambda - u_{1,0})^3} + \frac{\delta_2}{(\lambda - u_{2,0})^3}\right]^{-1}, \tag{24}$$

and the dissipation coefficient

$$\mathrm{C} = \mathrm{B}\left[\frac{\eta_{1,0}\delta_1}{(\lambda - u_{1,0})^3} + \frac{\eta_{2,0}\delta_2}{(\lambda - u_{2,0})^3}\right]. \tag{25}$$

Recall that c_2 is a kappa-dependent parameter related to quadratic nonlinearity in ϕ, which was defined earlier; see Equation (9) above.

It is interesting to point out that both the dispersion coefficient B and the damping coefficient C, given in Equations (24) and (25) above, respectively, may acquire negative values, due to an interplay between the values of the beam speeds $u_{1,0}$ and $u_{2,0}$ (and also $\eta_{1,0}$ and $\eta_{2,0}$, as regards C). This new possibility, nonexistent in beam-free plasmas—since, upon setting $u_{1,0} = u_{2,0} = 0$, both B and C become positive definite—calls for a certain caution in the physical interpretation of analytical solutions for physically meaningful quantities, such as, e.g., ϕ_1, governed here by Equation (22) above.

In the investigation that follows, we have considered a pair of proton (H^+) beams, i.e., consisting of identical microscopic particles (ions). Therefore, we may set $\eta_{1,0} = \eta_{2,0} = \eta_0$ to proceed. The dissipation coefficient is thus given by $\mathrm{C} = \eta_0/2$ (>0). Note that C is positive, therefore, throughout the remainder of the paper. However, B may either be positive (as in the beam-free case) or negative, depending on the value (s) of the beam speed(s) entering the expression (Equation (24)) above.

4.1. Symmetric Model

Let us consider a pair of counterpropagating beams of equal density and (absolute) drift velocity, by taking $\delta_1 = \delta_2 = 1/2$ and $u_{2,0} = -u_{1,0} = u_0$, along the lines introduced by Lakhina et al. (2020) and Verheest & Hellberg (2021). Equation (18) thus reduces to

$$\frac{1}{2(\lambda + u_0)^2} + \frac{1}{2(\lambda - u_0)^2} - \frac{\kappa - \frac{1}{2}}{\kappa - \frac{3}{2}} = 0, \tag{26}$$

which can be rewritten as

$$\frac{\lambda^2 + u_0^2}{(\lambda^2 - u_0^2)^2} - \left(\frac{\kappa - \frac{1}{2}}{\kappa - \frac{3}{2}}\right) = 0. \tag{27}$$

Two roots for λ^2 can be computed from the above biquadratic equation, in the form of

$$\lambda_F^2 = \frac{1}{2c_1}[1 + 2c_1u_0^2 + (1 + 8c_1u_0^2)^{1/2}] \tag{28}$$

and

$$\lambda_S^2 = \frac{1}{2c_1}[1 + 2c_1u_0^2 - (1 + 8c_1u_0^2)^{1/2}]. \tag{29}$$

From the above four roots thus obtained for $\lambda_{F,S}$, we shall retain the (two) positive roots for numerical analysis. Indeed, we need not discuss the case $\lambda < 0$, as it just follows the same behavior as $\lambda > 0$ in the symmetric case. It is straightforward to show that the latter two expressions could also be recovered from the dispersion relation (Equation (13)) in the small wavenumber limit, i.e., by assuming $k^2 \ll c_1$, viz. $\omega_0^2 \simeq k^2/c_1$ and setting $\lambda = \omega/k$ for the phase speed.

In this (symmetric) case, the nonlinearity, dispersion and dissipation coefficients in the KdVB equation can be respectively rewritten as

$$\mathrm{A} = \mathrm{B}\left\{\frac{3}{2}\left[\frac{1}{(\lambda + u_0)^4} + \frac{1}{(\lambda - u_0)^4}\right] - 2c_2\right\}, \tag{30}$$

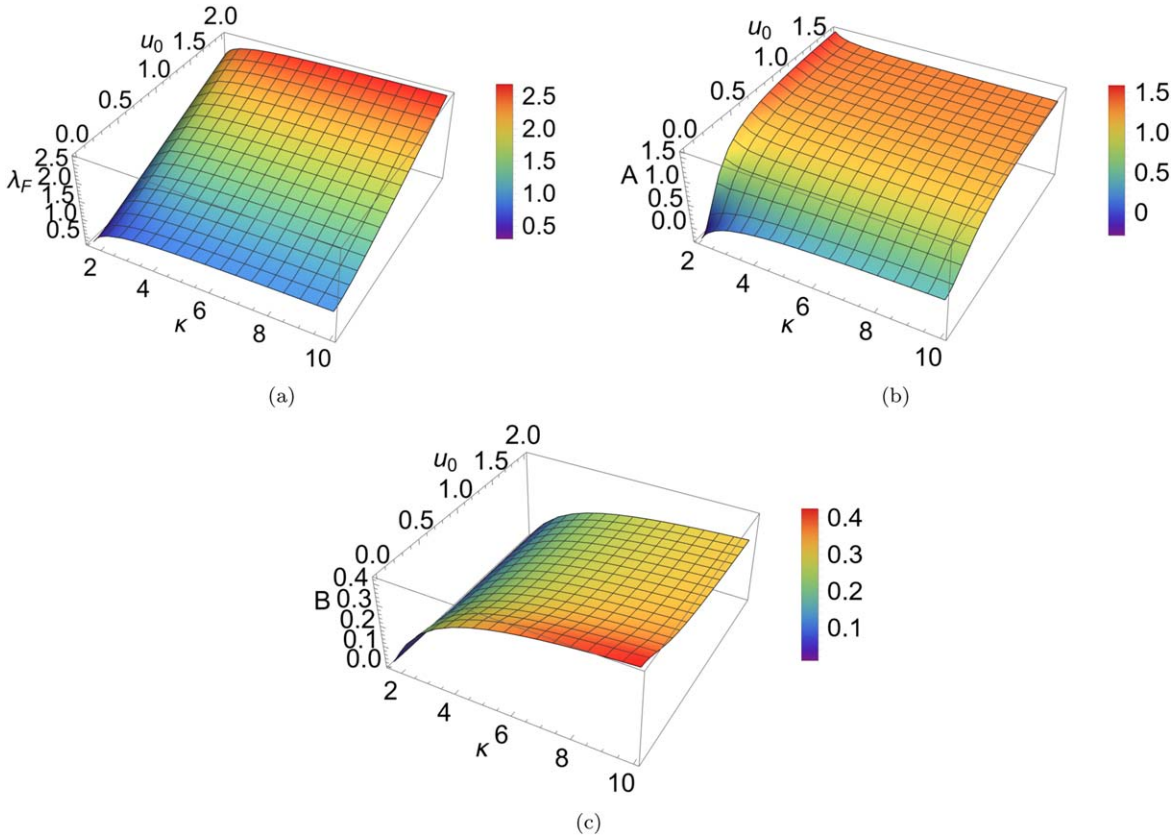

Figure 1. Symmetric case: fast mode. The variation of (a) the phase speed λ_F, based on Equation (28), (b) the nonlinearity coefficient A, and (c) the dispersion coefficient B with respect to κ and u_0. We have taken $\delta = 0.5$.

$$\mathrm{B} = \left[\frac{1}{(\lambda + u_0)^3} + \frac{1}{(\lambda - u_0)^3}\right]^{-1}, \tag{31}$$

and

$$\mathrm{C} = \eta_0/2. \tag{32}$$

Iterating an earlier comment, note that $\mathrm{C} > 0$, while B may either be positive (as in the beam-free case) or negative, depending on the value(s) of u_0 entering the expression (Equation (31)) above.

4.2. Asymmetric Model

We shall now consider a specific composition, by taking $\delta_1 = 2/3$, $\delta_2 = 1/3$, $u_{1,0} = -u_0$, and $u_{2,0} = 2u_0$. This ensures that the equilibrium is charge- and current-neutral, viz. $\delta_1 + \delta_2 = 1$ and $\delta_1 u_{1,0} + \delta_2 u_{2,0} = 0$. Equation (18) thus reduces to

$$\frac{2}{3(\lambda + u_0)^2} + \frac{1}{3(\lambda - 2u_0)^2} - \frac{\kappa - \frac{1}{2}}{\kappa - \frac{3}{2}} = 0, \tag{33}$$

which can be rewritten as

$$\lambda^4 - 2u_0\lambda^3 - \left(3u_0^2 + \frac{1}{c_1}\right)\lambda^2 + \left(4u_0^3 + \frac{2u_0}{c_1}\right)\lambda + \left(4u_0^4 - \frac{3u_0^2}{c_1}\right) = 0. \tag{34}$$

This quartic polynomial equation in λ has four roots. In this (asymmetric) case, the coefficients in the KdVB equation can be rewritten as

$$\mathrm{A} = \mathrm{B}\left[\frac{2}{(\lambda + u_0)^4} + \frac{1}{(\lambda - 2u_0)^4} - 2c_2\right], \tag{35}$$

$$\mathrm{B} = \frac{3}{2}\left[\frac{2}{(\lambda + u_0)^3} + \frac{1}{(\lambda - 2u_0)^3}\right]^{-1}, \tag{36}$$

and

$$\mathrm{C} = \eta_0/2. \tag{37}$$

We notice that, as in the symmetric case above, $\mathrm{C} > 0$ here too, while B may either be positive (as in the beam-free case) or negative, depending on the value(s) of u_0 entering the expression (Equation (36)) above.

4.3. Shock-wave Solution of the KdVB Equation

To obtain a stationary-profile solution of the KdVB equation, one may consider the variable transformation to the moving coordinate $\chi = \xi - \mathcal{V}\tau$ (while the variation, i.e., the derivative with respect to time τ will be suppressed). Here, λ is the speed of the electrostatic shock wave in the moving reference frame (i.e., moving at the sound speed), normalized by C_0; in other words, the shock speed will be equal to $v_{\mathrm{shock}} = \lambda + \epsilon\mathcal{V}$. Consider $\Phi = \phi_1(\xi, \tau)$, obeying Equation (22), which now becomes $\Phi(\chi)$ in the moving reference frame, whose dynamics

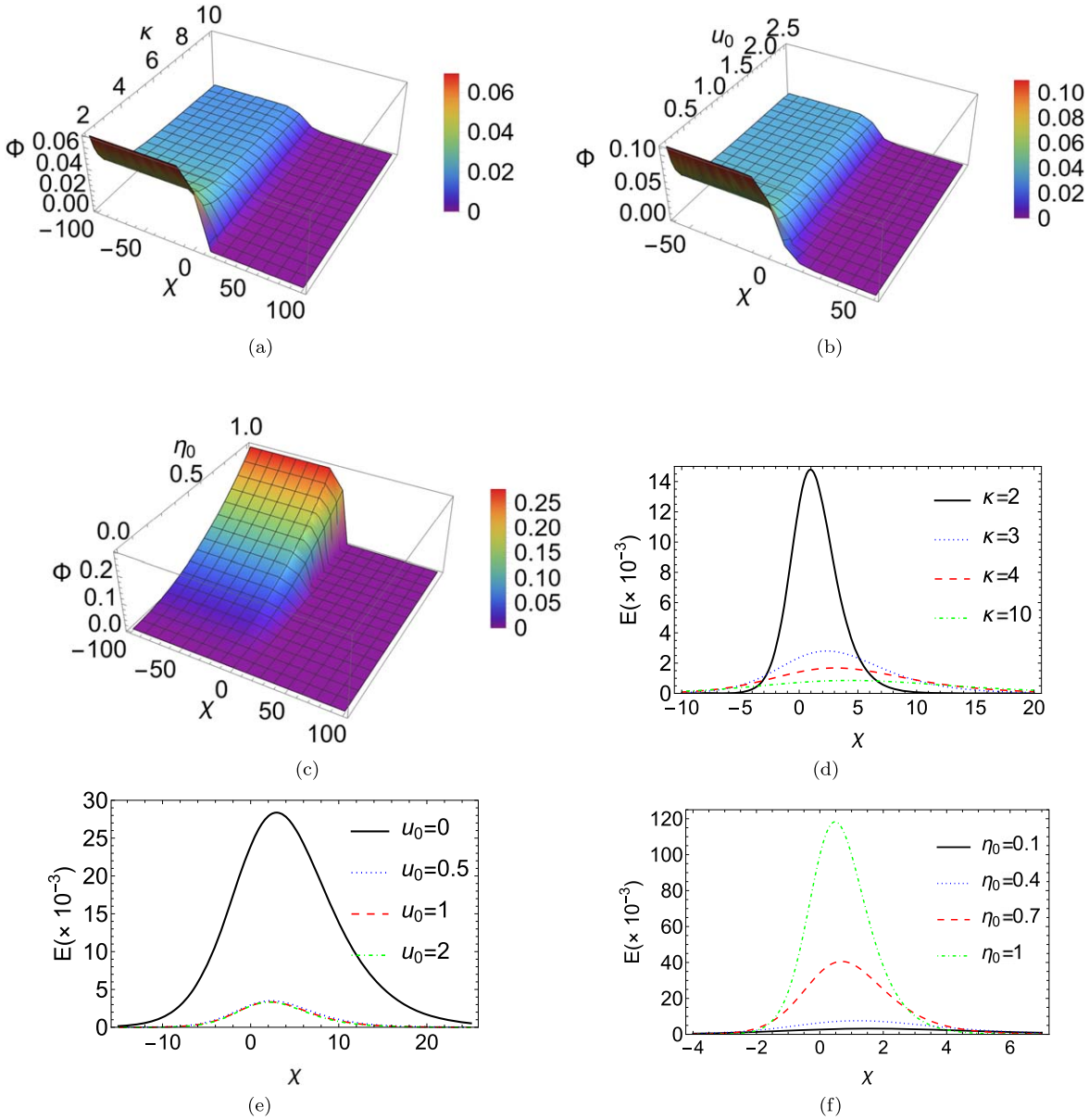

Figure 2. Symmetric case: fast mode. The variation of an electrostatic shock profile Φ is shown vs. χ, for different values of (a) the spectral index κ (for fixed $u_0 = 1.5$, $\eta_0 = 0.5$); (b) the beam velocity u_0 (for fixed $\kappa = 2$, $\eta_0 = 0.5$); and (c) the fluid viscosity η_0 (for fixed $\kappa = 2$, $u_0 = 1.5$). Furthermore, in panels (d), (e), and (f) the variation of the monopolar electric field (E) associated with the shock profiles corresponding to panels (a), (b), and (c), respectively, is depicted. We have taken $\delta = 0.5$ in these plots.

will obey the ordinary differential equation:

$$-\mathcal{V}\frac{d\Phi}{d\chi} + \mathrm{A}\Phi\frac{d\Phi}{d\chi} + \mathrm{B}\frac{d^3\Phi}{d\chi^3} = \mathrm{C}\frac{d^2\Phi}{d\chi^2}. \tag{38}$$

Kourakis et al. (2012b) revisited the well-known shock solutions of the KdVB equation, together with their limitations in the context of astrophysical plasma applications. The analytical solution of the KdVB equation can be found by using the hyperbolic tangent (tanh) method (Malfliet & Hereman 1996; Kourakis et al. 2012b; Sultana et al. 2012) to read

$$\Phi = \Phi_m\left\{1 - \frac{1}{4}\left[1 + \tanh\left(\frac{\chi}{\Delta}\right)\right]^2\right\}. \tag{39}$$

Here,

$$\Phi_m = \frac{3\mathrm{C}^2}{25\mathrm{AB}}$$

is the shock amplitude and

$$\Delta = \frac{1\mathrm{B}}{\mathrm{C}}$$

is related to the shock width, i.e., its spatial extension (the larger the value of Δ, the more stretched the shock form will be). Furthermore, the shock speed $\mathcal{V}$ is prescribed, as

$$\mathcal{V} = \frac{6\mathrm{C}^2}{25\mathrm{B}}.$$

We should point out that the shock excitation obtained for the electrostatic potential will be associated with a monopolar

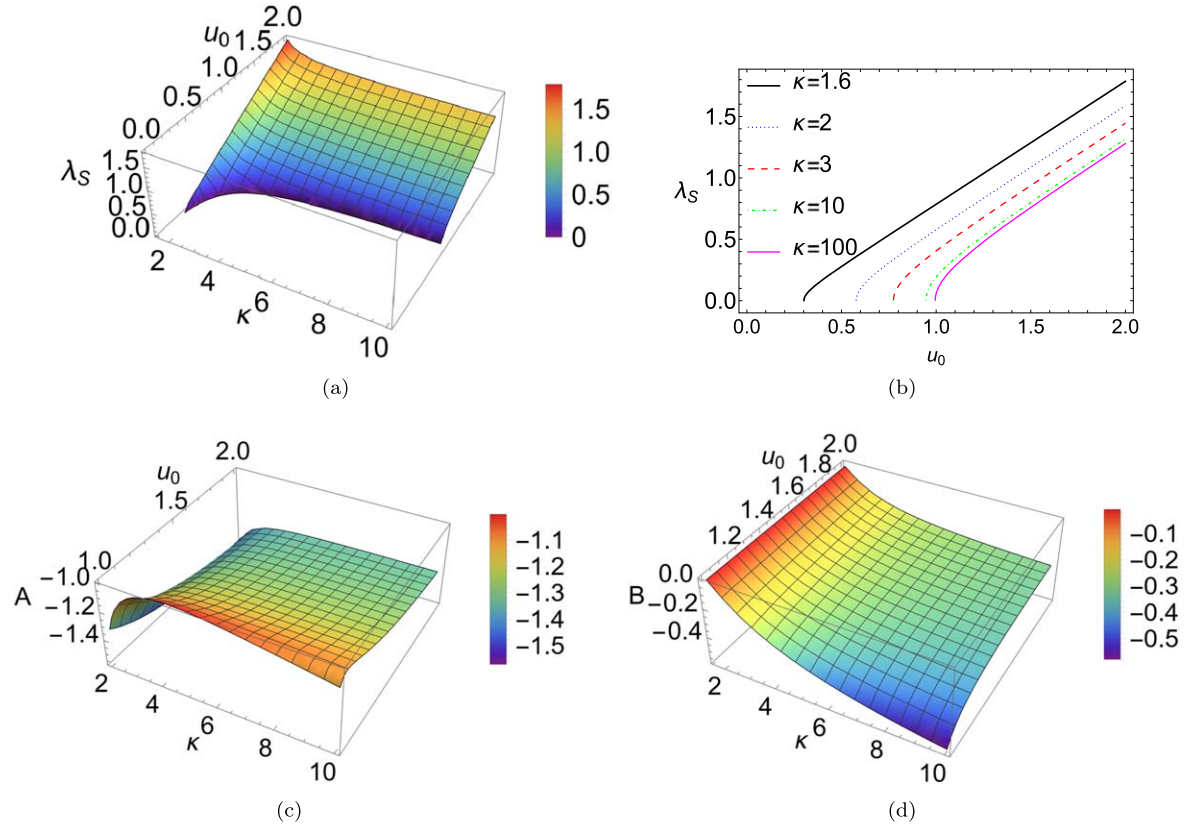

Figure 3. Symmetric case: slow mode. ((a), (b)) The variation of the phase speed λ_S, based on Equation (29); (c) the nonlinearity coefficient A, and (d) the dispersion coefficient B with respect to κ and u_0. We have taken $\delta = 0.5$. Note that the slow mode does not exist for u_0 values below a certain threshold, as illustrated in panel (b), hence the gap appearing in panel (a).

(pulse-like) form expected to be observed for the electric field. Recalling that $\boldsymbol{E} = -\nabla\Phi$ (in the electrostatic approximation), one obtains the following expression (in 1D geometry) for the E-field:

$$E = E_0\,\mathrm{sech}^2\left(\frac{\chi}{\Delta}\right)\left[1 + \tanh\left(\frac{\chi}{\Delta}\right)\right], \tag{40}$$

where $E_0 = \frac{\Phi_m}{2\Delta} = \frac{3C^3}{500AB^2}$ represents the maximum/minimum (for $A > 0$ or for $A < 0$, respectively) value of the monopolar E-field form. The former case ($E_0 > 0$) will be the standard case for IA waves ("positive polarity") in monopolar E-field space observations, while the latter case ($E_0 < 0$) will be referred to as a "negative polarity" excitation. This prediction matches, qualitatively speaking, certain space observations of propagating monopolar electric field waveforms (Tsurutani et al. 1998; De Keyser et al. 2010).

It is interesting to point out that, since all of the coefficients (A, B, and C) may be either positive or negative (see the discussion above), their sign may affect the sign(s) of Φ_m, Δ, and $\mathcal{V}$. As a consequence, different possibilities exist, as regards the shock behavior. Recall that $B > 0$ in the beam-free case; therefore, some of the possibilities open in our case did not exist in a beam-free model.

Let us assume that $\Delta > 0$. Note that the limit of RHS of Equation (39) for $\chi \to \mp\infty$ is Φ_m and 0, respectively, in this case. Therefore, the latter expression represents a positive-valued function, monotonically decreasing from $\Phi_m > 0$ to zero, for $AB > 0$.

On the other hand, the inverse monotonic behavior will be witnessed for $AB < 0$: a negative-valued function is obtained that increases from $\Phi_m < 0$ to zero as χ varies from $-\infty$ to ∞.

Inversely, assuming that $\Delta < 0$, the limit of RHS of Equation (39) for $\chi \to \mp\infty$ is 0 and Φ_m, respectively, in this case. Therefore, the latter expression represents a positive-valued function, monotonically increasing from zero to $\Phi_m > 0$, for $AB > 0$. On the other hand, for $AB < 0$, a negative-valued function is obtained that decreases from zero to $\Phi_m < 0$ as χ varies from $-\infty$ to ∞.

Interestingly, the sign of B determines the sign of the propagation speed $\mathcal{V}$ also: a positive B value (as in the beam-free case $u_0 = 0$) implies a rightward propagating excitation: an anti-kink soliton form is thus obtained if $A > 0$, while a kink soliton is obtained in $A < 0$. Inversely, a negative B value implies a leftward propagating excitation: however, a step-shaped function ($\Phi_m < 0$) propagating backwards is tantamount to an anti-kink propagating to the left (this is obvious, upon a space-reversal). Likewise, a descending-step-like function ($\Phi_m > 0$) propagating backward is tantamount to a kink excitation propagating to the left.

The different possibilities that exist in terms of our plasma parameters will be exposed in detail in Section 5.

5. Parametric Analysis

Based on the above algebraic results, we may now carry out a parametric investigation to study the characteristics of IA shocks associated with fast and slow modes in non-Maxwellian plasma.

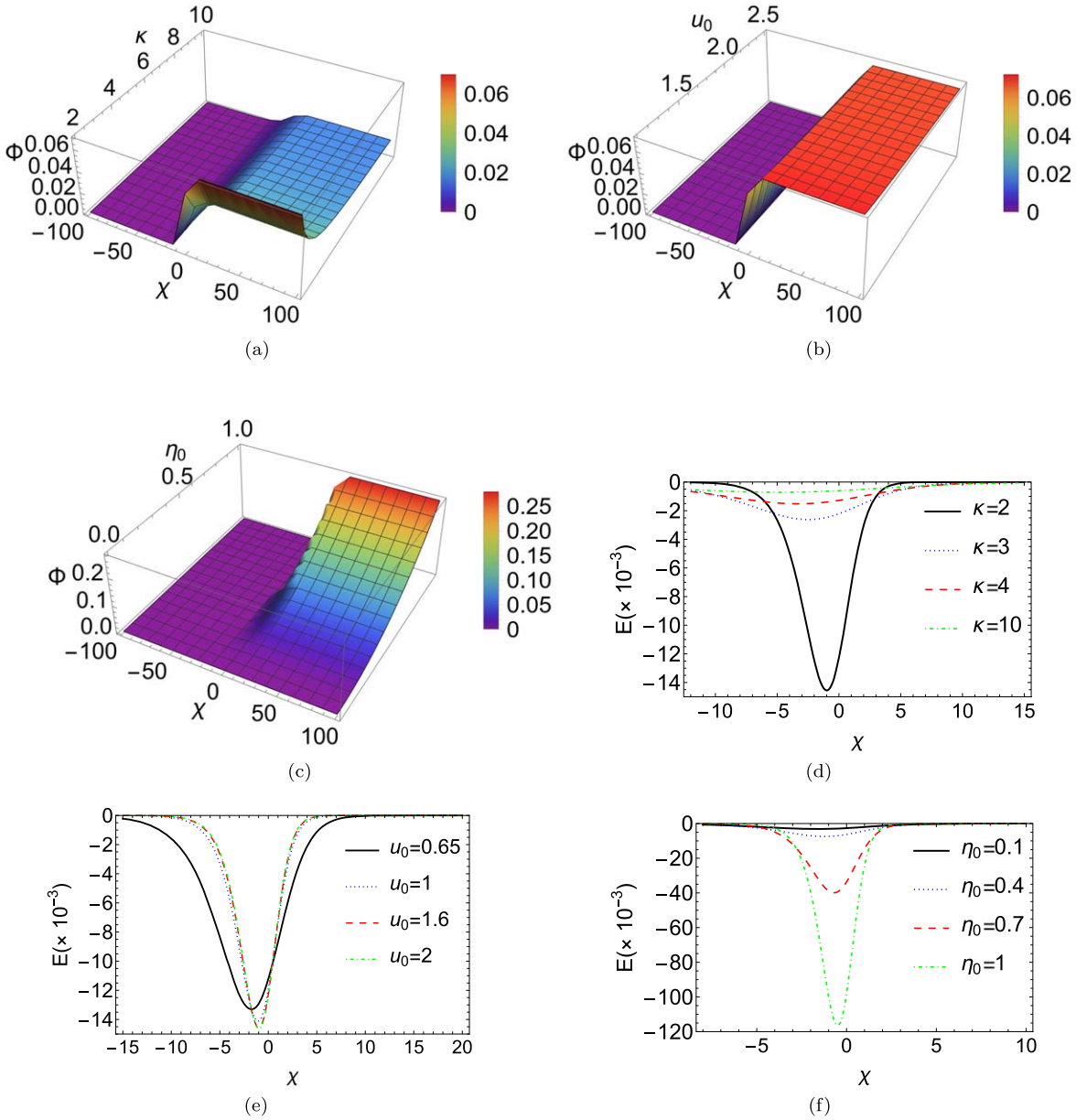

Figure 4. Symmetric case: slow mode. The variation of the shock profile Φ is shown vs. χ, for different values of (a) spectral index κ for fixed $u_0 = 1.5$, $\eta_0 = 0.5$; (b) beam velocity u_0 for fixed $\kappa = 2$, $\eta_0 = 0.5$; (c) fluid viscosity (η_0) for fixed $\kappa = 2$, $u_0 = 1.5$. Panels (d), (e), and (f) show the variation of the monopolar electric field profile (E) of the shock profiles corresponding to panels ((a), (b), (c)), respectively. We have taken $\delta = 0.5$.

5.1. Nonlinear Analysis

5.1.1. Symmetric Model

Fast mode. Figure 1 shows the dependence of (a) the phase velocity (λ_F) (i.e., the shock speed, to leading order), (b) the nonlinearity coefficient A, and (c) the dispersion coefficient B associated with the fast mode in a symmetric bi-ion-beam plasma, on the beam speed (u_0) and the electron spectral index (κ). Notice that all of the coefficients (A, B, and C) are *positive* in this case, which prescribes positive values of (all of) Φ_m, Δ, and $\mathcal{V}$ (see the definitions above). Note that the phase speed increases with either a larger beam velocity (value) or with a higher spectral index. In other words, stronger deviation from Maxwellian statistics (i.e., lower kappa) leads to a slower acoustic ("sound")—as expected from earlier works (Kourakis et al. 2012a)—and, consequently, to the possibility for a slower shock speed. An analogous effect regards the beam velocity, which actually seems to energize the shocks: the faster the beam, the faster a shock may be. It turns out that the nonlinearity coefficient (A) is slightly higher (for finite beam speed) for smaller κ (i.e., for stronger deviation from the Maxwellian), and also higher for higher beam speed (see Figure 1 (b)). Conversely, the dispersion coefficient decreases (slightly) for larger u_0, although it also decreases for smaller spectral index (value), as shown in Figure 1(c). Recall, in passing, that the dissipation coefficient in Equation (22) is directly proportional to the medium's viscosity (coefficient).

Figure 2 depicts an electrostatic shock profile associated with the fast mode, emphasizing its variation with different parameters. Note that only positive polarity (monopolar) electric field profiles associated with "shocks" (or anti-kink soliton forms) moving toward the right are predicted in this case, since both A and B are positive, for any u_0 and κ; see the definition of Φ_m in Equation (39). It is clearly seen that the

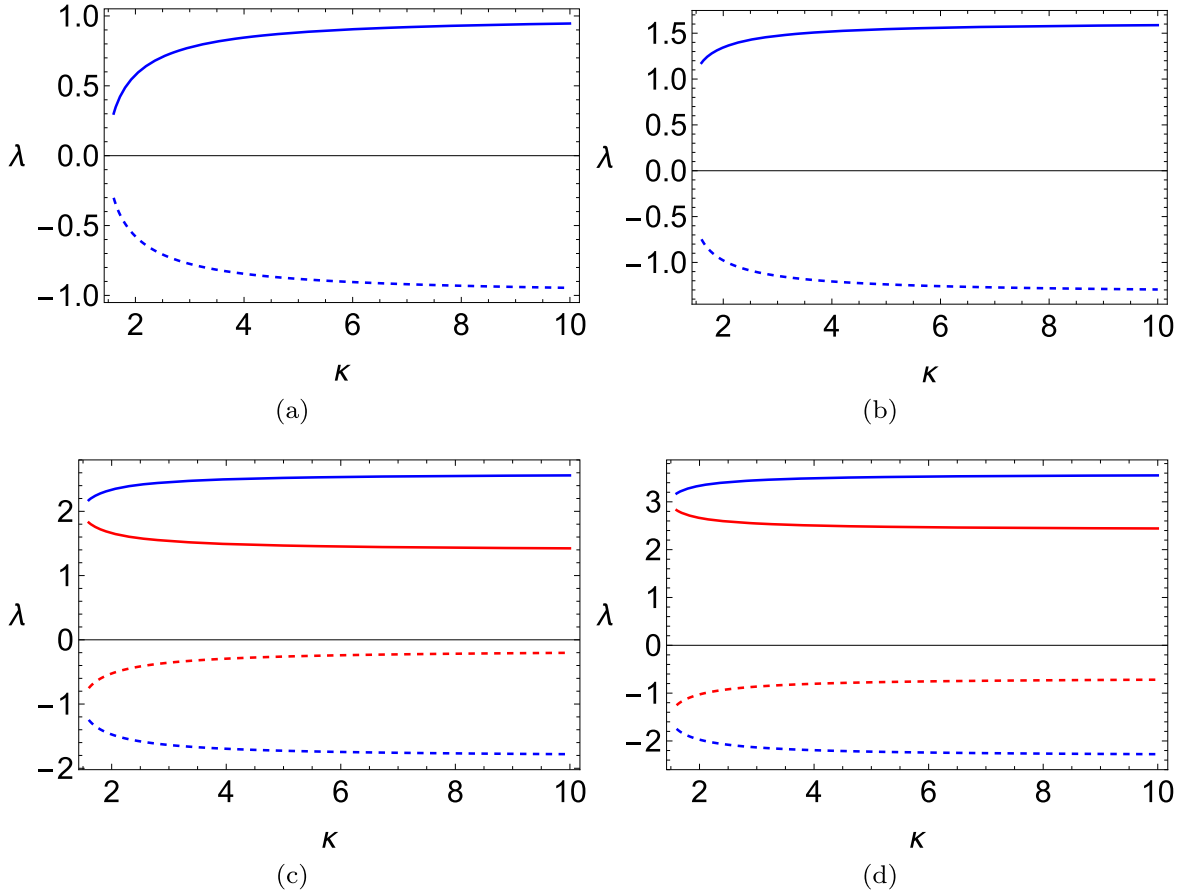

Figure 5. Asymmetric case. The phase velocity of the fast and slow mode(s) vs. the spectral index (κ), for (a) $u_0 = 0$; (b) $u_0 = 0.5$; (c) $u_0 = 1$; and (d) $u_0 = 1.5$, as well as for a fixed value of $\delta_1 = 2\delta_2 = 2/3$. The fast mode is shown in blue color and the slow mode is in red.

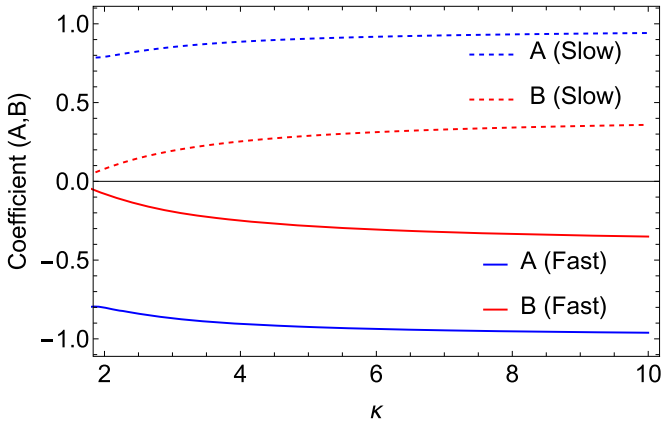

Figure 6. Asymmetric case. The variation of the coefficients A and B vs. the spectral index κ for the fast and the slow mode, respectively, are shown. In this plot, $\delta_1 = 2\delta_2 = 2/3$, $\eta_0 = 0.5$, and $u_0 = 1.5$ are kept fixed.

amplitude of IA shocks associated with the fast mode in the symmetric model decreases for higher values of either the spectral index and the beam velocity, as shown in panels (a) and (b), respectively. Lower values of kappa (i.e., stronger deviation from the Maxwellian behavior) will therefore result in stronger shocks. Note that larger amplitude shocks develop for higher values of viscosity coefficient, as seen in Figure 2(c): this is due to the amplitude being related to C^2, which in turn is directly proportional to η. Panels (d), (e), and (f) in the same figure illustrate the variation of the monopolar electric field (E) pulse profile of shocks corresponding to panels (a), (b), and (c), respectively.

Slow mode. Figure 3 depicts the variation of ((a), (b)) the phase speed (λ_S), (c) the nonlinearity coefficient A, and (d) the dispersion coefficient B, for electrostatic shocks associated with the *slow mode* in a symmetric bi-ion-beam plasma. Notice that coefficients A and B are both *negative* in this case (while $C > 0$), which prescribes positive values of Φ_m, but negative Δ and negative $\mathcal{V}$ (see the definitions above). Note that slow IA shocks only occur for values of the beam velocity exceeding a certain threshold value, as discussed in Singh et al. (2023). The phase speed increases for higher beam speed (value), and also for larger electron spectral index (kappa). Note that the nonlinear coefficient is negative for the slow mode. The absolute value of the nonlinear coefficient first decreases up to $\kappa \approx 4$ and then increases (see Figure 3(c)). We also notice that the nonlinearity coefficient increases in absolute value as the beam speed increases. The dispersion coefficient is also negative and increases (in absolute value) for larger u_0 and the spectral index as shown in Figure 3(d).

Figure 4 illustrates the variation of an electrostatic shock profile associated with the slow IA mode. Only negative polarity monopolar electric field profiles and anti-kink soliton forms (for ϕ) moving toward the left are observed, since B is negative in this case; see the definition of the propagation speed $\mathcal{V}$ following Equation (39).

One clearly sees that the amplitude of IA shocks associated with the slow mode in the symmetric model decreases for higher values of spectral index and beam velocity, as shown in panels

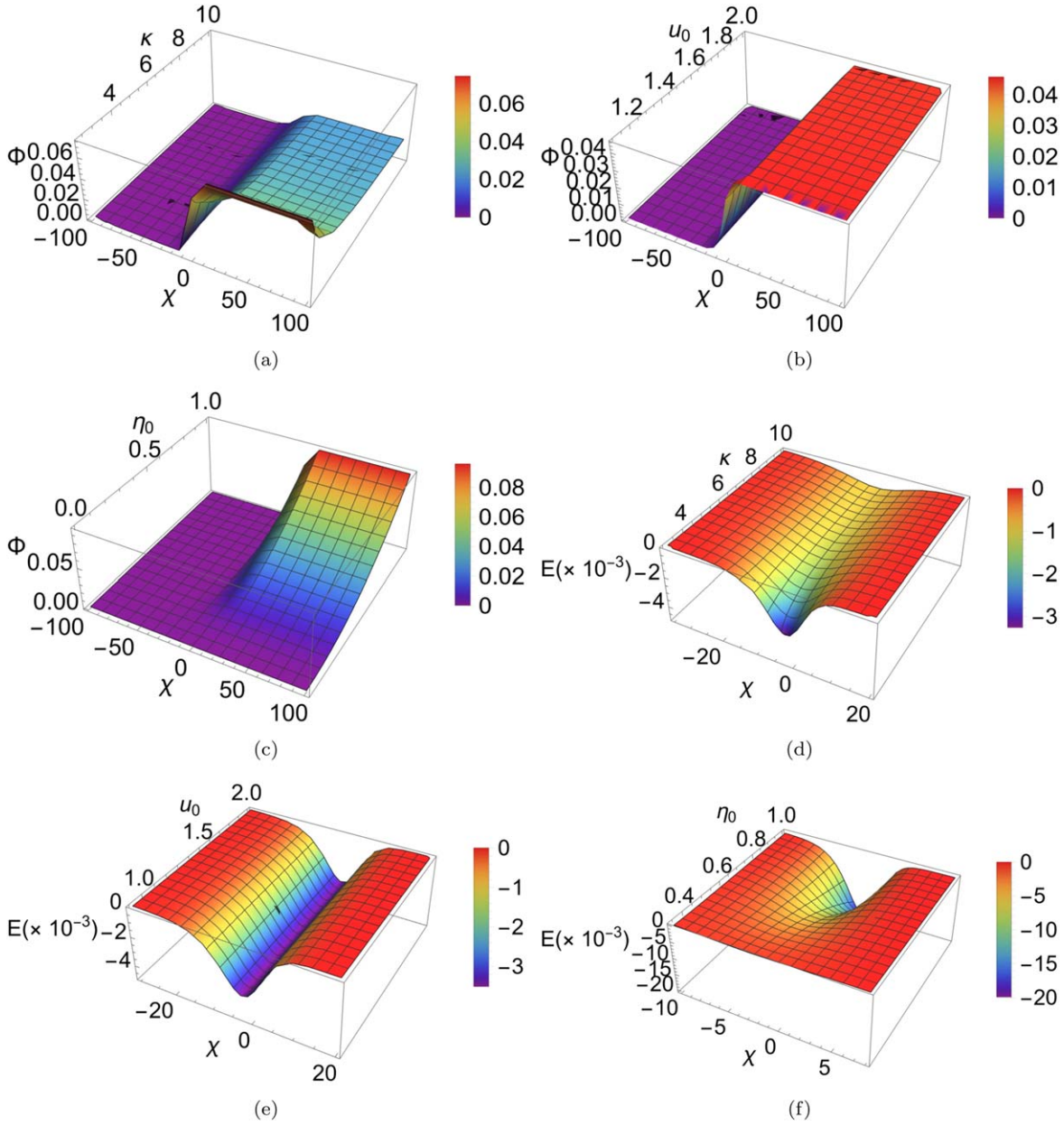

Figure 7. Asymmetric case: fast mode. The variation of the shock profile Φ vs. χ is shown, for different values of (a) spectral index κ for fixed $u_0 = 1.5$, $\eta_0 = 0.5$; (b) beam velocity u_0 for fixed $\kappa = 2$, $\eta_0 = 0.5$; and (c) fluid viscosity (η_0) for fixed $\kappa = 2$, $u_0 = 1.5$. Panels (d), (e), and (f) show the electric field (E) profile associated with the shocks depicted in panels (a), (b), and (c), respectively. Note that $\delta_1 = 2\delta_2 = 2/3$.

4(a) and (b), respectively. Note that larger amplitude IA shocks will evolve for high values of the viscosity coefficient, as shown in panel 4(c). Panels (d), (e), and (f) illustrate the variation of the monopolar electric field (E) pulse profile associated with the shocks shown in panels (a), (b), and (c), respectively.

5.1.2. Asymmetric Model

The variation of the phase speed (for both fast and slow modes) versus the spectral index of electron (κ) for different values of beam velocity is shown in Figure 5. Recall that only the fast mode exists below a certain threshold in the beam speed (value), as shown in Figure 5; see panels (a) and (b) therein. Above this threshold, both fast and slow modes may occur in the κ domain. Conversely to the previous case (slow mode), the fast mode phase speed increases for lower κ (see Figures 5(c) and (d)), i.e., for stronger deviation from the Maxwellian picture.

Figure 6 shows the variation of the nonlinearity (A) and dispersion (B) coefficients versus the spectral index (kappa), for a fixed value of the beam speed. Note that both coefficients are negative for the fast mode and positive for the slow mode.

Fast mode. Notice that the coefficients A and B are both *negative* in this case (while $C > 0$), which prescribes positive values of Φ_m, but negative Δ and negative $\mathcal{V}$ (see the definitions above). Figure 7 illustrates the variation of an IA shock profile associated with the fast mode. Only negative polarity electric field profiles associated with shocks (or anti-kink solitons) moving toward the left are observed, since $B < 0$ in this case; note the definition of the propagation speed $\mathcal{V}$ following Equation (39). We see that the amplitude of IA shocks associated with the fast mode in the symmetric model

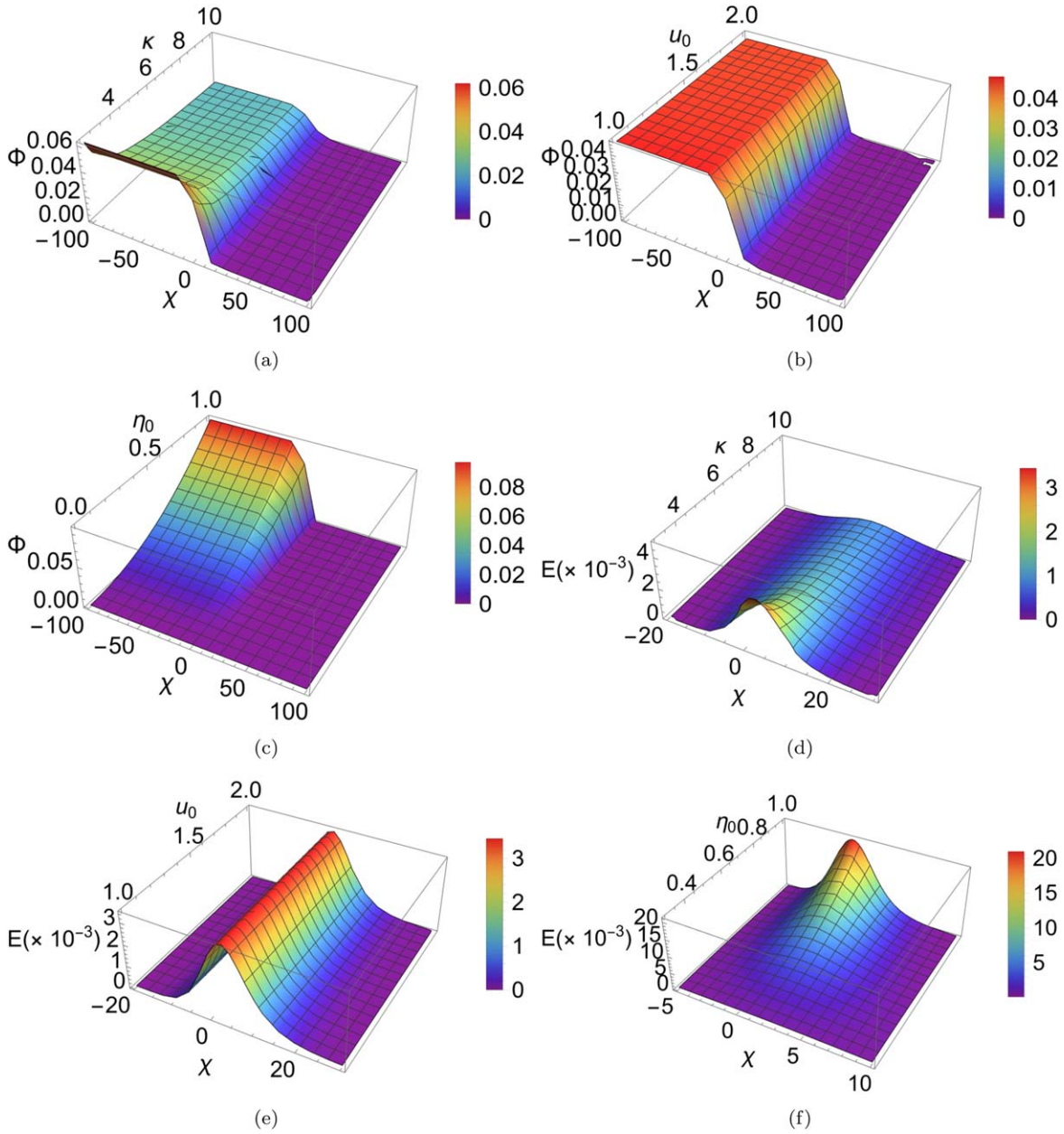

Figure 8. Asymmetric case: slow mode. The variation of the shock profile Φ vs. χ is shown, for different values of (a) spectral index κ for fixed $u_0 = 1.5$, $\eta_0 = 0.5$; (b) beam velocity u_0 for fixed $\kappa = 2$, $\eta_0 = 0.5$; and (c) fluid viscosity (η_0) for fixed $\kappa = 2$, $u_0 = 1.5$. Panels (d), (e), and (f) show the electric field profile (E) of shocks corresponding to panels (a), (b), and (c). Note that $\delta_1 = 2\delta_2 = 2/3$.

decreases for higher values of either the spectral index or beam velocity as shown in panels (a) and (b), respectively. Note that large amplitude IA shocks will evolve for high values of the viscosity coefficient given in panel (c). The last three panels ((d), (e), (f)) in the same figure show the variation of the monopolar electric field (E) pulse profile associated with the potential forms depicted in panels (a), (b), and (c), respectively.

Slow mode. Notice that all coefficients A, B, and C are *positive* in this case, which prescribes positive values of (all of) Φ_m, Δ, and $\mathcal{V}$ (see their definitions above). Figure 8 illustrates the variation of IA shock profiles associated with the slow mode. Only positive polarity electric field profiles associated with shocks (or anti-kink solitons) moving toward the right are observed, since $B > 0$ in this case; note the definition of the propagation speed $\mathcal{V}$ following Equation (39). We see that the amplitude of IA shocks associated with the slow mode in the symmetric model decreases for higher values of either the spectral index or the beam velocity, as shown in Figure 8(a) and (b), respectively. Note that large amplitude IA shocks will evolve for high values of the viscosity coefficient, as shown in panel (c) in the same figure. Panels (d), (e), and (f) show the variation of monopolar electric field pulse profile (E) of shocks corresponding to panels (a), (b), and (c), respectively.

6. On the Occurrence of Shocks in Earth's Magnetotail: Prediction from First Principles

Drawing inspiration from the observations of Liu et al. (2019) in reconnection jet regions in Earth's magnetotail, we have considered two cold counterstreaming ion beams with non-Maxwelian electrons. We have adopted the plasma parameters reported in the latter reference. The concentration

Table 1
The Characteristics of IA Shock Waves Have Been Computed by Using the Data Sets Listed in Liu et al. (2019)

S. No	Mode	Distribution	V (km s^{-1})	ϕ (V)	$\lvert\Delta\rvert$ (km)	E (mV m^{-1})
1	Fast IA mode	$\kappa_e = 2$	1102	120	4.3	15
	parallel to B	$\kappa_e = 20$	1212	−18	21	−0.6
2	Slow IA mode	$\kappa_e = 2$	790	118	4.4	−14
	parallel to B	$\kappa_e = 20$	675	−14	23	0.34
3	Fast IA mode	$\kappa_e = 2$	−1156	400	6.7	−31
	antiparallel to B	$\kappa_e = 20$	−1340	−526	33	0.1
4	Slow IA mode	$\kappa_e = 2$	−638	542	7.2	41
	antiparallel to B	$\kappa_e = 20$	−453	−5.72	36	−0.1

Note. The concentration of the first proton beam I is $n_1 = 2.6 \times 10^4$ m^{-3}, while its streaming velocity is $u_1 = -900$ km s^{-1}. The concentration of the second proton is $n_2 = 0.9 \times 10^4$ m^{-3}, with streaming velocity $u_2 = 950$ km s^{-1}. The electron concentration is $n_e = 3.5 \times 10^4$ m^{-3}, with temperature $T_e = 2.86$ keV. The IA sound speed for these values (in e-i plasma) is $C_S = 523$ km s^{-1} and the Debye length is $\lambda_{De} = 2.12$ km. Note that we considered viscosity $\eta_0 = 0.5$. Here, ϕ is the shock amplitude (in volts), V is the phase speed (in kilometers per second), and $|\Delta|$ is the width of shocks (in kilometers).

of the first proton beam I is $n_1 = 2.6 \times 10^4$ m^{-3}, while its streaming velocity is $u_1 = -900$ km s^{-1}. The concentration of the second proton is $n_2 = 0.9 \times 10^4$ m^{-3}, with streaming velocity $u_2 = 950$ km s^{-1}. The electron concentration is $n_e = 3.5 \times 10^4$ m^{-3}, with temperature $T_e = 2.86$ keV. The IA sound speed for these values (in e-i plasma) is $C_S = 523$ km s^{-1} and the Debye length is $\lambda_{De} = 2.12$ km. Thus, the dimensionless parameters in our model take the values $\delta_1 = 0.74$, $\delta_2 = 0.26$, $U_1 = -1.72$, and $U_2 = 1.82$. Note that we have considered viscosity $\eta_0 = 0.5$ (as an arbitrary, indicative value).

The signatures of electrostatic waves propagating antiparallel to the ambient magnetic field $\boldsymbol{B}$ that were observed by the MMS spacecraft in the reconnection jet region, as reported by Liu et al. (2019), with potential $\phi \sim$ (50–200) V, velocity antiparallel to $\boldsymbol{B} = -650$ km s^{-1} and width $\Delta \sim 20$ km. Table 1 presents the attributes of both fast and slow modes of IA shock waves corresponding to parallel (antiparallel) waves relative to the magnetic field. Our findings demonstrate good agreement with the findings reported by Liu et al. (2019).

In this work, we have introduced an analytical framework modeling the occurrence of shock waves, with implications in the reconnection jet regions in Earth's magnetotail. In summary, our observations suggest that streaming beams, suprathermal electrons, and fluid viscosity combined could bear a significant impact on the existence and also on the propagation characteristics of subsonic waves in the reconnection jet region of the magnetotail. Notwithstanding the (limited) disparity in the (value of the) velocity of the fast mode—in comparison with the observations reported by Liu et al. (2019)—the predicted amplitude and phase velocity falls within an acceptable magnitude range. This is true, particularly, in the direction parallel to the magnetic field. It is worth noting that Liu et al. (2019) exclusively detected signals of electrostatic nonlinear waves with an *antiparallel* orientation.

The results of this fundamental investigation, from first principles, is in good agreement with the observations of nonlinear excitations in the reconnection jet region(s) in Earth's magnetotail that were reported by Liu et al. (2019) and may be further confirmed by some future space missions.

7. Conclusions

We have investigated the existence domains for both fast and slow IA subsonic shock waves in suprathermal space plasma comprising two counterstreaming (drifting) ion beams with non-Maxwellian (suprathermal) electrons. We have employed a perturbative technique to derive an evolution equation in the form of a hybrid KdVB type PDE for the electrostatic potential. Our ambition was to shed some light on the role of the beam velocity and the spectral index on the evolution of subsonic shock waves and also on their potential existence in the magnetotail.

We have considered, separately, two cases, namely a symmetric beam pair, and also an asymmetric case (of two different beams). In both of these cases, for beam velocity above the threshold, both supersonic as well as subsonic waves may exist. Note that only positive polarity monopolar electric field profiles—associated with shocks of anti-kink soliton shape—moving toward the right (i.e., in the positive direction) are predicted, for the symmetric fast mode and—independently—for the asymmetric slow mode. Inversely, only negative polarity electric field (monopolar) profiles—associated with shocks of anti-kink soliton shape—moving toward the left (i.e., in the positive direction) are found for the symmetric case fast modes and also—independently—in the asymmetric case slow modes. The combined effects of the beam velocity (value) and electron superthermality on the characteristics of subsonic shock waves have been analyzed. Both symmetric and asymmetric models are considered to explore the evolution of subsonic shock waves in non-Maxwellian plasma.

The findings of this investigation should help elucidate the—mostly unexplored—characteristics of subsonic shock waves observed in the magnetosphere. Our investigation establishes the possible occurrence of subsonic shocks inside reconnection jets of Earth's magnetosphere (Liu et al. 2019; Lakhina et al. 2021; Singh et al. 2023), based on observations by Liu et al. (2019).

Acknowledgments

The authors acknowledge financial support from Khalifa University's Space and Planetary Science Center under grant No. KU-SPSC-8474000336. They also gratefully acknowledge financial support from Khalifa University (Abu Dhabi, UAE) via project FSU-2021-012/8474000352 as well as a CIRA (Competitive Internal Research) CIRA-2021-064/8474000412 grant.

Data Availability

Any data that support the findings of this study are included within the article. No new data were created or analyzed in this study.

ORCID iDs

Kuldeep Singh https://orcid.org/0000-0003-3526-8085
Frank Verheest https://orcid.org/0000-0001-6800-5789
Ioannis Kourakis https://orcid.org/0000-0002-4027-0166

References

Andersson, L., Ergun, R. E., Delory, G. T., et al. 2015, SSRv, 195, 173
Armstrong, T. P., Paonessa, M. T., Bell, E. V., & Krimigis, S. M. 1983, JGR, 88, 8893
Baboolal, S., Bharuthram, R., & Hellberg, M. A. 1990, JPlPh, 44, 1
Berthomier, M., Pottellete, R., & Malingre, M. 1998, JGR, 103, 4261
Boström, R., Gustafsson, G., Holback, B., et al. 1988, PhRvL, 61, 82
Bryant, D. A. 1996, JPlPh, 56, 87
Cao, J., Ma, Y., Parks, G., et al. 2013, JGRA, 118, 313
Chen, G., Fu, H. S., Zhang, Y., et al. 2019, ApJL, 881, L8
De Keyser, J., Maggiolo, R., & Echim, M. 2010, AnGeo, 28, 2027
Dubinov, A. E. 2009, PlPhR, 35, 991
Ergun, R. E., Carlson, C. W., McFadden, J. P., et al. 1998, GeoRL, 25, 2041
Feldman, W. C., Asbridge, J. R., Bame, S. J., Montgomery, M. D., & Gary, S. P. 1975, JGR, 80, 4181
Fu, H. S., Vaivads, A., Khotyaintsev, Y. V., et al. 2017, GeoRL, 44, 37
Gingell, I., Schwartz, S. J., Eastwood, J. P., et al. 2019, GeoRL, 46, 1177
Graham, D. B., Khotyaintsev, Y. V., Vaivads, A., & Andre, M. 2015, GeoRL, 42, 215
Heinrich, H., Kim, S. H., & Merlino, R. L. 2009, PhRvL, 103, 115002
Hellberg, M. A., Mace, R. L., Baluku, T. K., Kourakis, I., & Saini, N. S. 2009, PhPl, 16, 094701
Hellberg, M. A., & Verheest, F. 2008, PhPl, 15, 062307
Ho, G. C., Starr, R. D., Gold, R. E., et al. 2011, P&SS, 59, 2016
Kakad, A., Kakad, B., Anekallu, C., et al. 2016, JGRA, 121, 4452
Kakad, B., Kakad, A., Aravindakshan, H., & Kourakis, I. 2022, ApJ, 934, 126
Kirk, J. G., & Skjaeraasen, O. 2003, ApJ, 591, 366
Kourakis, I., Sultana, S., & Hellberg, M. A. 2012a, PPCF, 54, 124001
Kourakis, I., Sultana, S., & Verheest, F. 2012b, Ap&SS, 338, 245
Lakhina, G. S., Singh, S. V., Kakad, A. P., & Pickett, J. S. 2011, JGRA, 116, A10218
Lakhina, G. S., Singh, S. V., & Rubia, R. 2020, PhyS, 95, 105601
Lakhina, G. S., Singh, S. V., & Rubia, R. 2021, AdSpR, 68, 1864
Lazar, M., Schlickeiser, R., Poedts, S., & Tautz, R. C. 2008, MNRAS, 390, 168
Leubner, M. P. 1982, JGR, 87, 6335
Liu, C. M., Vaivads, A., Graham, D. B., et al. 2019, GeoRL, 46, 12702
Livadiotis, G. 2018, EL, 122, 50001
Livadiotis, G., & McComas, D. J. 2014, JPlPh, 80, 341
Livadiotis, G. 2017, Kappa Distributions: Theory & Applications in Plasmas (Amsterdam: Elsevier)
Mahmood, S., & Ur-Rehman, H. 2013, JPSJ, 82, 074501
Malfliet, W., & Hereman, W. 1996, PhyS, 54, 563
Matsumoto, H., Kojima, H., Miyatake, T., et al. 1994, GeoRL, 21, 2915
Mendis, D. A., & Rosenberg, M. 1994, ARA&A, 32, 419
Nakamura, Y., Bailung, H., & Shukla, P. K. 1999, PhRvL, 83, 1602
Norgren, C., Andre, M., Vaivads, A., & Khotyaintsev, Y. V. 2015, GeoRL, 42, 1654
Pickett, J. S., Chen, L. J., Kahler, S. W., et al. 2004, AnGeo, 22, 2515
Pickett, J. S., Kurth, W. S., Gurnett, D. A., et al. 2015, JGRA, 120, 6569
Sagdeev, R. Z. 1966, in Reviews of Plasma Physics, ed. M. A. Leontovich, 4 (New York: Consultants Bureau), 23
Singh, K., Kakad, A., Kakad, B., & Saini, N. S. 2021, MNRAS, 500, 1612
Singh, K., Kakad, A., Kakad, B., & Saini, N. S. 2021, EPJP, 136, 14
Singh, K., Kakad, A., Kakad, B., & Kourakis, I. 2022, A&A, 666, A37
Singh, K., Varghese, S. S., Verheest, F., & Kourakis, I. 2023, ApJ, 957, 96
Sultana, S., Sarri, G., & Kourakis, I. 2012, PhPl, 19, 12310
Tsurutani, B. T., Arballo, J. K., Lakhina, G. S., et al. 1998, GeoRL, 25, 4117
Ur-Rehman, H., Mahmood, S., & Ur-Rehman, A. 2014, PhyS, 89, 105605
Varghese, S. S., Singh, K., & Kourakis, I. 2024, MNRAS, 527, 8337
Vasyliunas, V. M. 1968, JGR, 73, 2839
Verheest, F., & Hellberg, M. A. 2009, in Handbook of Solitons: Research, Technology and Applications, ed. S. P. Lang & S. H. Bedore (Hauppauge, NY: Nova Science Publishers, Inc.), 353
Verheest, F., & Hellberg, M. A. 2021, PhyS, 96, 045603
Washimi, H., & Taniuti, T. 1966, PhRvL, 17, 996
Yamada, M., Kulsrud, R., & Ji, H. 2010, RvMP, 82, 603
Zhou, Z., Wei, F., Feng, X., et al. 2018, ApJ, 863, 84